Improving interruption performance of mechanical circuit breakers by controlling pre-current-zero wave shape

Author(s):
Schultz, Tim [ID]; Hammerich, Benjamin; Bort, Lorenz [ID]; Franck, Christian [ID]

Improving interruption performance of mechanical circuit breakers by controlling pre-current-zero wave shape

Tim Schultz[1] ✉, Benjamin Hammerich[1], Lorenz Bort[1], Christian M. Franck[1]

[1]High Voltage Laboratory, ETH Zurich, Physikstrasse 3, 8092 Zurich, Switzerland
✉ E-mail: tsc@ethz.ch

Abstract: Mechanical circuit breakers (MCBs) are the limiting component for current injection HVDC circuit breakers. Improving their interruption performance reduces requirements for capacitance and inductance needed in the injection circuit and thus space use and costs. Higher performance can be achieved by creating a period of low current gradient before zero crossing in the MCB, e.g. by using a saturable inductor (SI). In this paper, the impact of duration and steepness during the low current-gradient phase is linked to arc parameters of the investigated model gas circuit breaker. It is shown in a scaled experimental setup that an optimum design of the SI can be derived from arc time constant and interruption limits for constant current gradients. This optimisation results in a considerable increase of interruption performance. The feasibility of implementing an SI in a full-scale HVDC circuit breaker is demonstrated using simulations. Using an improved injection scheme, the stresses for the MCB can be reduced significantly. Consequently, the injection circuit components can be scaled down, making the topology more economical. The reduced interruption requirements might also make it possible to use a single gas interrupter instead of a series connection of vacuum interrupters, reducing the complexity of the mechanical switch.

1 Introduction

The safe and reliable operation of multiterminal high voltage DC (HVDC) grids requires a sophisticated protection system. The interruption requirements in such systems differ fundamentally from HVAC grids [1, 2]. Due to the absence of a current zero crossing, fault currents in HVDC systems cannot be interrupted by mechanical circuit breakers (MCBs) alone. Additionally, the converters in HVDC systems are considerably less tolerant to surge currents than AC transformers. For typical HVDC systems, this requires fault neutralisation times in the single digit millisecond range [2]. While power electronic switches can easily meet these requirements, their on-state losses are considerably higher than those of mechanical switches.

To cope with these requirements, a large number of circuit breaker topologies with different properties has been proposed [3–8]. The vast majority of these breakers consists of three parallel paths, the nominal current path (NCP), the current commutation path (CCP) and the energy absorption path (EAP). In the closed state, the current is conducted via the NCP, either using an ultra-fast disconnector or a MCB, which is optimised for low conduction losses. In case of a fault, the current is commutated into the CCP, where the counter voltage is build up to stop the current flow. Overvoltages due to inductive energy, which is stored in the system, are limited by the surge arrester (SA) elements in the EAP.

If an MCB is used, an artificial current zero crossing has to be generated in the NCP within a short time. To realise this, an active current injection scheme can be used. In this case, the CCP consists of a pre-charged capacitor, an inductor and an activation switch. Once the fault is detected and the MCB in the NCP has reached a sufficient contact separation, the activation switch is closed, initiating a current flow through the NCP in the opposite direction, eventually leading to a current zero crossing.

A key factor for the interruption performance of a current injection topology is the mechanical opening time as well as the interruption capability of the MCB [8]. Using a switch with shorter mechanical operation time, the peak current can be limited and thus stresses on equipment reduced. Additionally, a high interruption capability of MCBs, i.e. the ability to successfully interrupt faults with high current gradients before and high voltage gradients after zero crossing, allows to reduce capacitance and inductance in the

injection circuit and thus minimise cost. Due to their high voltage withstand capability for small gap distances and high interruption capability compared to gas circuit breakers (GCBs) [1], vacuum circuit breakers (VCBs) can be used [2, 9, 10]. However, VCBs are limited in their voltage withstand. In AC, they are typically used in medium voltage applications. In recent years, research has pushed these boundaries and first results for single-break prototypes for voltages above 100 kV have been published [11, 12]. For the proposed operating voltages in future HVDC grids, however, a series connection of VCBs is required, which comes at the cost of mechanical complexity. GCBs have superior dielectric properties, which is the reason for their dominance in high voltage applications. For a GCB, a single unit would be sufficient, however at the cost of having a larger LC circuit to cope with the lower interruption capability.

Interruption limits (for GCBs and VCBs) depend on both current profile before and voltage profile after current zero. The current before zero crossing determines the conductance of the arc plasma and thus the probability of interruption and reignition after zero crossing, when voltage builds up. For a successful interruption, a low conductance of the plasma at and after current zero is desired.

For this reason, attempts have been made to reduce current gradient immediately before zero crossing. A promising option is the use of a saturable inductor (SI) in series with the MCB. For currents above a certain threshold, the SI is in saturation and thus has a low inductance. When the current approaches zero shortly before the interruption, the core of the SI de-saturates, drastically increasing its inductance. This reduces the rate of rise of current shortly before zero crossing (RRC_{CZ-}) to decrease the stresses for the MCB. Additionally, the rate of rise of voltage after current zero (RRV_{CZ+}) is reduced by the additional inductance.

The idea to improve interruption performance by adding a SI in series with the MCB has already been around in an early phase of the development of HVDC circuit breakers [9, 13–16]. Greenwood and Lee [3] discussed the effects of reducing both rate of rise of current before and rate of rise of voltage after zero crossing on a theoretical basis. Experimental data supporting the hypothesis that a SI influences the interruption performance of VCBs has been published by several authors [13, 14, 17, 18]. A comprehensive study by Yanabu *et al.* [14] shows the impact of different SIs on
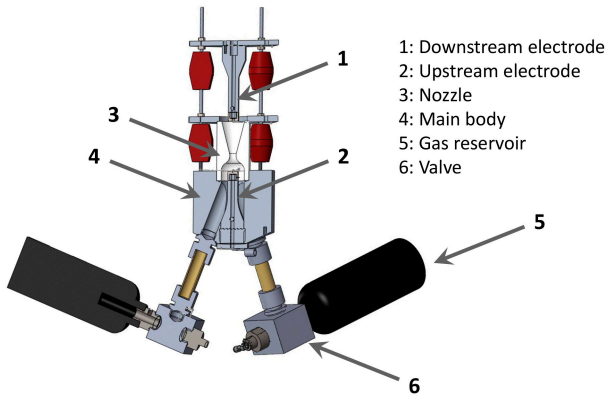
Fig. 1 *Model GCB used in the presented study [23]*

1: Downstream electrode
2: Upstream electrode
3: Nozzle
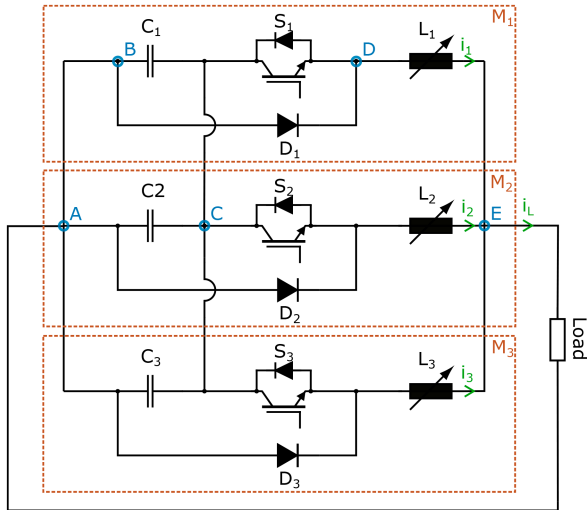4: Main body
5: Gas reservoir
6: Valve

Fig. 2 *Flexible pulsed current source used for investigating arc time constant [25]*

rate of change of current and voltage around zero crossing. Findings of Niwa *et al.* [17] also allude that the duration of the period of low current gradient has an impact on the interruption performance of VCBs.

By using experimental methods, this paper shows that performance improvement is possible for GCBs as well. With the obtained data, arc time constant and interruption performance for constant current gradients can be linked to the interruption performance when introducing a period of low current gradient before zero crossing. It is demonstrated that an optimum design of the SI for GCBs can be derived from that, once arc time constant and interruption performance for constant current gradients are known.

Based on the experimental findings, an optimised current injection topology employing a SI is presented. Using simulations, the feasibility of the design for HVDC systems as well as its advantages compared to a regular LC injection circuit are illustrated. Using the described system, the necessary capacitance in the current injection circuit can be minimised and the costs reduced.

2 Dynamic characteristics of the arc

The interruption performance of a GCB is dependent on various, complex processes in the arcing chamber. Of major importance is conductance and thus geometry and temperature profile of the arc. This is largely influenced by gas flow and energy exchange between arc plasma and surrounding material, e.g. ohmic heating, radiative and convective cooling as well as nozzle ablation. In steady-state conditions, heating and cooling are balanced. For current interruption, a zero crossing, i.e. a changing current, is required, and during this transient change of current, heating and cooling are not balanced. With decreasing current, the ohmic

heating changes, as well as the cooling due to changes in temperature profile and geometry of the arc. However, these changes are not instantaneous, and each of the cooling mechanisms can be associated with a time constant, describing the inertia of the respective process (e.g. change of plasma or wall temperature, decrease of arc radius) [19, 20].

As a consequence, the success of interruption is not only dependent on the current gradient at zero crossing (or any other single point in time), but rather on the development of the current in a certain period before zero crossing. The same applies for the voltage after zero crossing. The duration of this time period is dependent on heat balance and thus on the time constants of the specific GCB design that is investigated. In case the current (voltage) is linear for the relevant period, interruption performance can be related to the rate of change of current (voltage) before (after) current zero, as is commonly done in AC applications [21, 22].

Cao and Stokes [19] find that the dominant time constant can be attributed to radiative cooling. Consequently, if the current slope can be decreased before current zero for a duration in the range of this time constant, the interruption performance can be expected to increase. If the period of low current gradient lasts for five times the time constant or longer, the interruption performance is assumed to be comparable to a linear current with the same gradient (as an exponential transition process is assumed).

2.1 Model GCB

In the presented study, a model GCB was used, which is depicted in Fig. 1. It consists of a set of fixed arcing contacts, embedded in a nozzle. A gas flow for cooling is established by discharging three gas reservoirs into the arcing chamber. For the conducted tests, air at a pressure of 6 bar is used. The arc is initiated by an ignition wire.

### 2.2 Experimental method to determine the arc time constant

To determine the arc constant under relevant low current conditions, a flexible pulsed direct current source is used [24, 25] (cf. Fig. 2). This consists of three independent buck converter modules that can control their output current by applying the output voltage across a pre-set inductor.

To determine the time constant of the model GCB, a quasi-constant current is generated by one module to set the operating point, using the maximum inductance of 4.5 mH. The arc is then excited using current pulses of triangular shape, generated by a second module with 0.2 mH as inductance. The third module is not used. To achieve falling current slopes (which are solely determined by load voltage and module inductances) that are similar to the rising slopes, a $1.3\,\Omega$ resister was placed in series with the model GCB, and the charging voltage of the capacitors was reduced to 2000 V. The voltage across and current through the model GCB for an example measurement is illustrated in Fig. 3.

The evaluation of the arc time constant is based on a generalised Mayr model for a dynamic arc (cf. (1)) [26]. In this equation, $g(t)$ describes the arc conductance, τ its dominant time constant, $i(t)$ the current and $u(t)$ the voltage. $P(g)$ is the cooling power, which is considered to be a function of the conductance (as opposed to be constant in [26]). Due to the limited excitation from the operating point and the low duration of the current pulses, the arc time constant is considered constant and the cooling power is considered to be linear with the conductance

$$\frac{\dot{g}(t)}{g(t)} = \frac{1}{\tau}\left(\frac{i(t) \cdot u(t)}{P(g)} - 1\right) \tag{1}$$

To determine the linearised $P(g)$ relationship, two fix points are needed. One can be found in the steady state before the current pulse is injected. The second fix point for $P_{max}(g_{max})$ as well as τ are determined using a least square error optimisation, comparing to the conductance based on measured current and voltage.
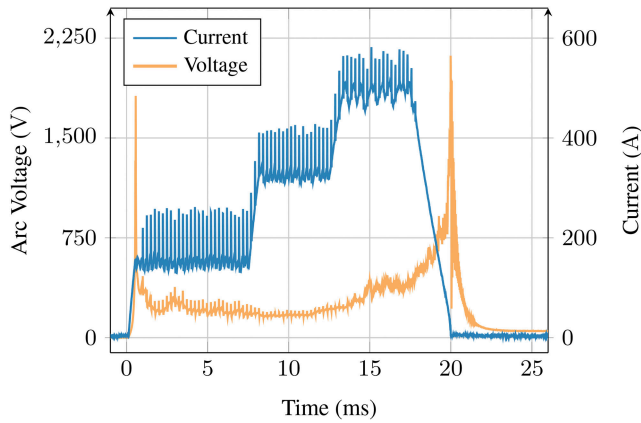
**Fig. 3** *Current and arc voltage during measurement to determine arc constant Δt*

a

b
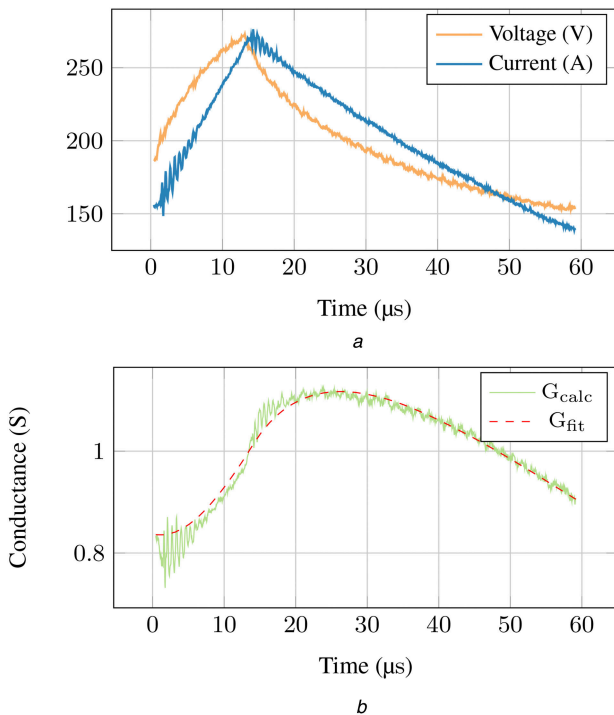
Fig. 4 *Close-up of a single spike, used to determine arc time constant τ*
(a) Measured current and voltage of a representative current spike, *(b)* Conductance calculated from measured current and voltage (G_{calc}) and fitted using the described algorithm (G_{fit})

### 2.3 Arc time constant for the tested model GCB

Fig. 4*a* illustrates the current through the model GCB during a single current spike as well as the arc voltage and the resulting conductance. The current measurement is used to determine τ with the described algorithm.

As expected, the injected current shows a steep, quasi-linear rise of about 8.8 A μs^{-1} for ∼10 μs. The oscillations that accompany the beginning of rise, peak and end of the injected current are caused by the switching operation of the used semiconductors. The ripple introduced by the two switching actions has a small amplitude and high frequency compared to spike and thus is expected not to influence the results. Comparing current and conductance, it becomes apparent that the arc diverges from its static voltage–current characteristic, as peak conductance is reached about 10 μs after peak current. This indicates that the selected parameters for the injected current are reasonable.

The distribution of the resulting time constants from all spikes at ∼140 A base current, the lowest available current level, is illustrated in Fig. 5. The distribution is centred around 5–6 μs. This compares reasonably well to investigations by Cao and Stokes [19], who determined a median of 4.75 μs for an ablation arc with a
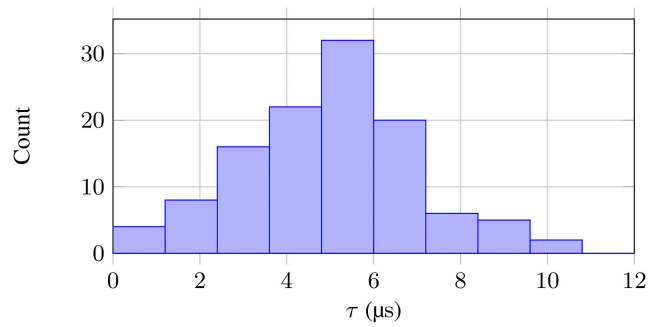
Fig. 5 *Histogram of the calculated arc time constant τ for a base current of 140 A from a total of 115 spikes*
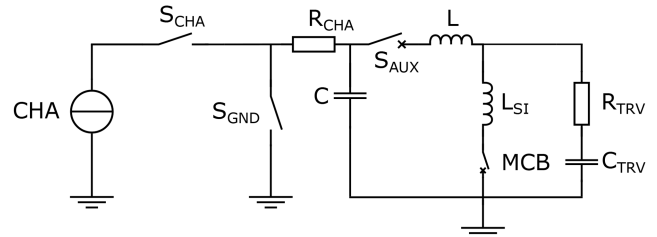
Fig. 6 *Setup to determine interruption performance of MCB, including a adjustable air core reactor (L) and a tuneable SI (L_{SI})*

similar length in PTFE. Chapman and Jones find similar values, ranging from 3.5 to 10 μs using an air blast circuit breaker [20]. Other sources also find values in the few microsecond range [27–29]. Considering the exponential characteristic of the process, this means that the arc would take about 25–30 μs (5τ) to adapt fully to the new conditions, if current instantaneously changes from one value to another. Similarly, the interruption performance of different wave shapes should be comparable, as long as the current is kept at a common trajectory for a duration of at least $5 \cdot \tau$ before zero crossing (taken that voltage after current zero crossing develops identically).

3 Interruption performance test circuit

To determine the interruption capability of the model GCB, an LC test circuit is used (cf. Fig. 6). Amplitude and arc duration can be influenced by adapting inductance, capacitance and pre-charge voltage. In parallel to the device under test, a snubber circuit is connected that can be used to influence the rate of rise of voltage after interruption. More information regarding the setup and used GCB can be found in [23].

Both the inductance of the air coil inductor (L) and of the SI (L_{SI}) can be adjusted by changing the number of turns and, for the SI, the air gap in the core.

4 Design of the SI

To verify the assumption that the arc fully adjusts to new conditions within 5τ, the impact of the current wave shape shortly before zero crossing needs to be investigated. For that purpose, a SI is developed and a test bench is used to compare the interruption performance of the model GCB for currents with and without an additional period of low current gradient.

The design of the SI is focused on reducing (di/dt) that exceeds the interruption capability of the GCB to a value below the threshold for successful interruption for the optimum time duration. This is visualised qualitatively in Fig. 7, using a simplified two-state model. The saturation current (I_{sat}) marks the level, above which the SI acts as an air coil. Consequently, in this region, the rate of change of current (di/dt_{sat}) is high. Below saturation current, inductance of the coil increases considerably, leading to a period of low current gradient ($di/dt_{non-sat}$) with a duration Δt to facilitate interruption at current zero.
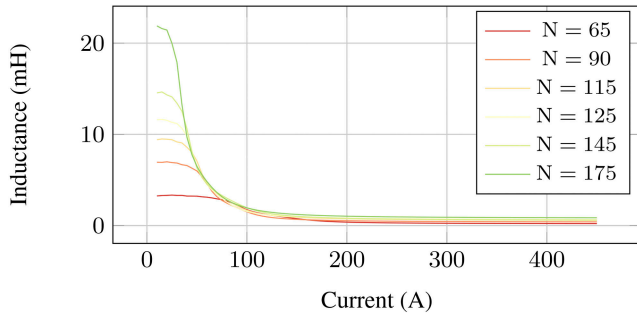
As discussed, the duration of the period of low current gradient needs to be sufficiently long for the arc to adjust to the new
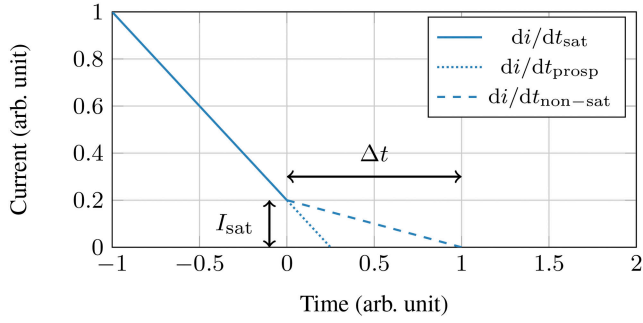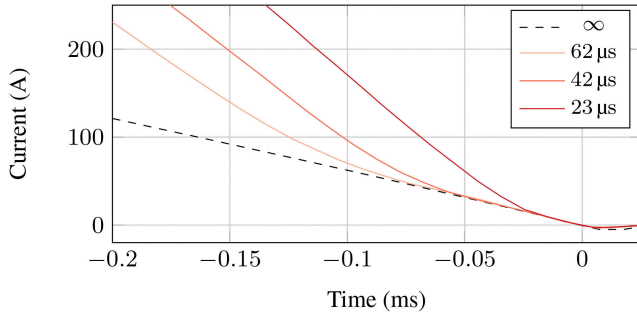
Fig. 7 *Influence of SI on current in the MCB. I_{sat}: saturation current of SI, Δt: period of low current gradient*

Table 1 Parameters of the SI

Component	Value
N	35–225
A_E	30 cm²
δ	0.1–4 cm
B_S	1.5 T

Fig. 8 *Example of the inductance characteristic of the designed SI as a function of current for different number of connected turns for fixed air gap ($\delta = 10\,mm$)*

Fig. 9 *Design verification: parameter variation of Δt, while keeping $di/dt_{non-sat}$ and di/dt_{sat} fixed*

conditions, characterised by the arc time constant (τ). However, increasing the duration of this phase requires a higher saturation current, which in turn requires a larger inductor core volume, increasing space use and costs. To determine the ideal duration of the period of low current gradient for the model GCB, a flexible inductor design is required.

4.1 Dimensioning

The rate of rise of current in the MCB when clearing a fault in a current injection circuit breaker at zero crossing is defined by the superposition of fault and injection current. The injection current is the result of the pre-charged capacitor discharging into the inductance of the CCP (and NCP) branch. If the arc voltage is neglected, it can be assumed proportional to the capacitor voltage divided by the loop inductance

$$di/dt_{MCB} = \frac{u_c(t_{CZ})}{L} + di/dt_{fault} \quad (2)$$

Here, u_c is the injection capacitor voltage and L is the loop inductance.

In the test circuit, described in Section 3, this corresponds to the voltage across the capacitor divided by the sum of L and L_{SI}.

The inductance of a SI in the non-saturated state can be approximated for a single-layer coil by using the following formula:

$$L_{SI,\,non-sat} = \frac{\mu_0 A_E N^2}{\delta + l_E(\mu_0/\mu_E)} \quad (3)$$

Here, A_E is the core cross-section, N the number of turns, δ the air gap length, l_E length of the magnetic path in the core and μ_E the core permeability. The saturation current for a core material with the saturation flux B_S is given by

$$I_{sat} = \frac{N B_S A_E}{L} = \frac{B_S \delta}{N \mu_0} \quad (4)$$

The period of low current gradient can be approximated by

$$\Delta t = \frac{I_{sat}}{di/dt_{non-sat}} \quad (5)$$

From these equations, a dimensioning can be derived for a specific set of parameters (di/dt_{sat}, $di/dt_{non-sat}$, Δt).

4.2 Design verification

In the presented case, a tapped inductor with adjustable air gap is selected to be able to realise a variety of combinations regarding mentioned parameters. For a more compact and economic design, a multi-layer coil is used (Table 1).

Using a power choke tester (ed-k DPG10-1000A), the designed inductor is characterised. A number of example measurements with varied parameters is illustrated in Fig. 8. Adjusting air gap and number of turns makes it possible to set saturation current and unsaturated inductance value over a wide range.

A side effect of changing the number of turns is that the inductance of the coil is not only changed in the non-saturated, but also in the saturated state. To avoid an undesirable influence on the rate of rise during high currents (di/dt_{sat}) when changing from linear inductor to SI, an adjustment of the linear inductance in the test circuit can be performed.

While the transition between non-saturated and saturated region happens in a rather narrow window, it is still not ideal and immediate. Hence, for the definition of the duration of the period of low current gradient, a transition point has to be defined (i.e. the saturation current). In this paper, the current that corresponds to an inductance value in the middle between non-saturated and saturated state is used (cf. (6))

$$L_{SI}(I_{sat}) = \frac{L_{SI,\,non-sat} + L_{SI,\,sat}}{2} \quad (6)$$

The period of low current gradient can then be defined as the time between reaching the saturation current and current zero crossing. While different definitions are possible (e.g. reaching 90% of the non-saturated inductance value), they do not impact the general trends presented in this paper.

Fig. 9 illustrates example measurements using the described SI and the LC test circuit. This example shows that using the correct settings, it is possible to conduct variations of one of the three parameters (in this case Δt), while keeping the other two ($di/dt_{non-sat}$ and di/dt_{sat}) fixed.
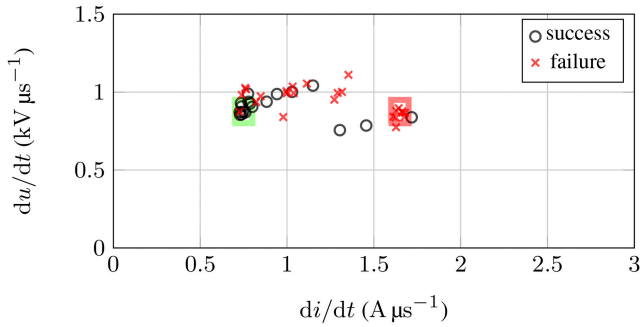
Fig. 10 *Interruption performance of test MCB for constant current gradients, failure region: red box, success region: green box*
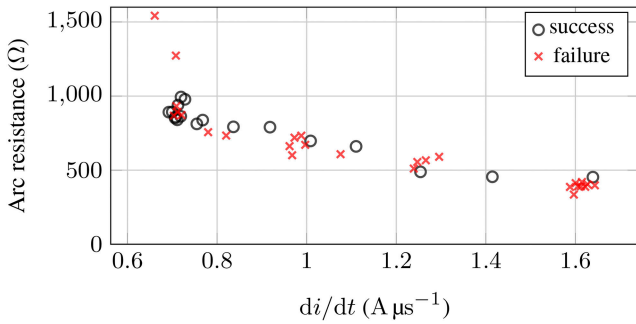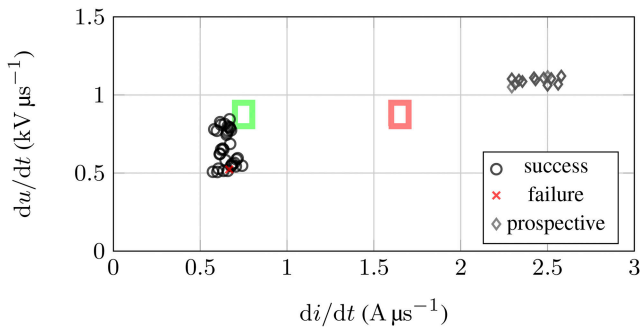

Fig. 11 *Arc resistance 500 ns before zero crossing as a function of RRC_{CZ-} at zero crossing*

Fig. 12 *Improvement of MCB interruption performance when using a SI, prospective: expected values at current zero if inductor would remain in saturation, obtained by simulation (no period of low current gradient), green/red box: success/failure region of linear inductor tests (cf. Fig. 10)*

5 Interruption capability

In the following, the interruption capability of the model GCB with and without SI are investigated. Using the performance for constant current gradients as a reference, the impact of the SI on interruption performance of the model GCB can be determined.

5.1 Linear inductor

In the presented test cases with linear inductor, the success of interruption is determined by the rate of rise of current before zero (RRC_{CZ-}) and the rate of rise of voltage after zero (RRC_{CZ+}). As a linear inductor is employed, the RRC_{CZ-} can be considered constant around zero crossing. Here, it is determined by a linear fit of the last 20 μs before zero crossing. The rate of change of voltage after interruption is determined by linear fitting the voltage between zero crossing and 75% of the recovery voltage peak. For a fixed RRC_{CZ+}, interruption will always be successful if the RRC_{CZ-} is below a certain value and always fail if it is above a second threshold. In between, a transition happens.

Fig. 10 shows experimental results for interruption tests with RRC_{CZ+} in a limited range (0.8–1.1 kV μs^{-1}) and a variation of RRC_{CZ-} over a wide range (0.7–1.7 A μs^{-1}). The boxes illustrate two regions with a very high chance of interruption (success

region, green) and failure (failure region, red), respectively. In between, the described transition between both modes occurs.

The impact of RRC_{CZ-} on the interruption performance results from the difference in energy input in the arc plasma before zero crossing. Higher rate of rise of current corresponds to higher currents before zero crossing and thus increased heating power and energy input that has not (completely) been dissipated at current zero. Consequently, the arc is more conductive at that time instant, which increases the chance of failure to interrupt.

Fig. 11 illustrates the arc resistance shortly before current zero as a function of RRC_{CZ-} for the measurements presented in Fig. 10. The resistance is calculated from measured arc voltage and current and is averaged over the range from 450 to 550 ns before current zero to reduce the impact of noise. As expected, a negative correlation between arc resistance shortly before interruption and rate of change of current can be seen. Apart from two outliers, this trend is almost linear and also confirms the increased chance of failure for lower arc resistances shortly before zero crossing.

5.2 Saturable inductor

The two regions identified using the linear inductor (cf. Fig. 10) serve as a reference for the SI. Using the adjustable inductor described in Section 4, a parameter study is conducted. The parameters are selected in a way that the prospective values for RRC_{CZ-} and RRC_{CZ+} (without de-saturation of the SI) exceed the failure region to make sure that interruption criteria are not met. Saturation current and non-saturated inductance are set to create periods of low current gradient of variable duration with a fixed and decreased di/dt that is slightly below the limit for successful interruption determined with the linear inductor.

Fig. 12 shows the results of the interruption tests using a SI in series with the MCB. The current gradients in saturated and non-saturated state are fixed in a narrow range. A comparison with Fig. 10 shows that the SI design successfully reduced the RRC_{CZ-} from beyond the failure region (prospective values) to the success region. Additionally, the RRC_{CZ+} was considerably reduced. This is a result of the increased inductance in the MCB branch. The voltage build-up after current interruption is governed by charging of the stray capacitance of the MCB through the loop inductance. Using the SI, this inductance is increased considerably, reducing the charging currents and consequently the RRC_{CZ+}.

As a result, the stresses for the MCB can be reduced and the chance of interruption increased. This confirms that the positive effect of the SI, previously demonstrated for VCBs, can also be seen for GCBs.

The resistance of the arc shortly before current zero crossing is often used as an indicator for the thermal interruption performance of GCB [30]. The corresponding values for the interruption tests with the SI are depicted in Fig. 13 as a function of Δt, keeping the di/dt in high current and low current period constant between the measurements, as illustrated in Fig. 9. As expected, the values positively correlate with Δt for short duration of the period of low current gradient. In contrast, if Δt exceeds a certain value, a further extension of the duration of low current gradient does not have an impact on the arc resistance shortly before zero crossing. A comparison with Fig. 11 shows that the arc resistance for long Δt is in the same range as when using a linear inductor (di/d$t_{CZ-} \simeq 0.7$ Aμs^{-1}, $R_{arc} \simeq 900\,\Omega$). Consequently, it is not expected to influence the interruption capability. The threshold between the two areas appears to be at approximately $t_{trans} \simeq 30 - 40\,\mu$s. Furthermore, a comparison between the arc resistance for long Δt with the respective values for employing a linear inductor only (cf. Fig. 11) shows a good correspondence.

The development of the arc resistance supports the assumption that, if the current slope before zero crossing is changed, a transition between the conditions for the high current di/dt and the low current di/dt happens. The minimum duration for a full transition (t_{trans}), which can be used as a design parameter to reduce the size of the required inductor, is similar to the expected duration, derived from the measurement of the thermal time constant (5τ).
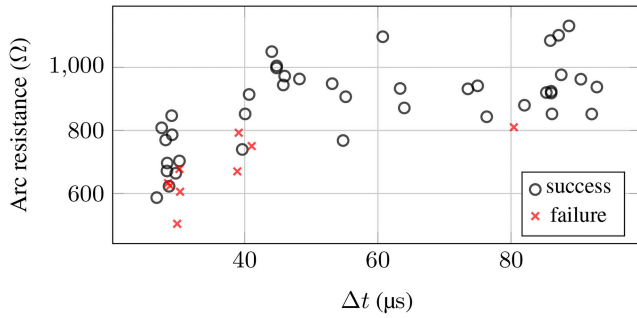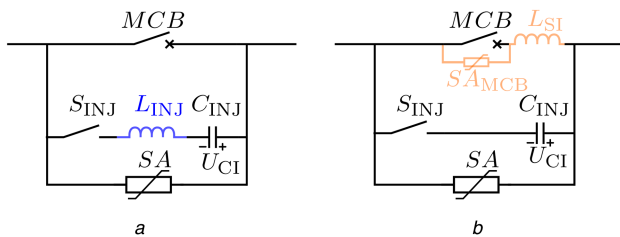
Fig. 13 *Arc resistance as a function of Δt for $di/dt_{sat} \simeq 0.7\,A\,\mu s^{-1}$ and $di/dt_{non-sat} \simeq 2.3\,A\,\mu s^{-1}$*

a

b
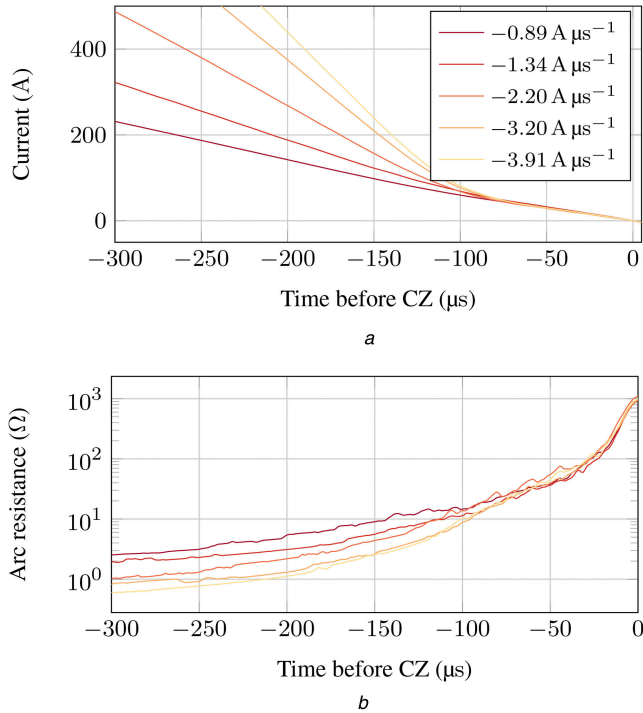
Fig. 14 *Impact of a variation of the gradients in the high current period (di/dt_{sat}) on arc resistance for fixed gradient during low current period ($di/dt_{non-sat} \simeq 0.7A\,\mu s^{-1}$)*

(a) Development of current before zero crossing, *(b)* Arc resistance before current zero crossing

Fig. 15 *Equivalent circuit diagram of current injection circuit breakers for HVDC applications*

(a) Reference topology (Ref), *(b)* Improved injection (Imp)

The independence of the high current phase on the interruption performance for long enough period of low current gradient is further supported by the results presented in Fig. 14. In this series of experiments, Δt and $di/dt_{non-sat}$ are kept constant and the slope in the high current regime is varied. The substantial difference between the rate of change of current in both phases is clearly visible. The development of current and arc resistance is depicted for several hundred microseconds before zero crossing. While the resistance differs considerably at the high current phase, it converges during the period of low current gradient to values with

a considerably decreased relative difference close to current zero, as expected.

6 Simulation of improved current injection circuit breakers for HVDC networks

To evaluate the feasibility of using SIs with the presented design criteria in current injection circuit breaker topologies for HVDC networks, a simulational study is conducted.

6.1 Topology and dimensioning of components

Fig. 15 depicts the differences between current injection circuit breakers with reference (Ref, black and blue elements) and improved injection topology (Imp, black and orange elements). Typically, a capacitor (C_{INJ}) that is pre-charged to system voltage is used together with a linear inductor (L_{INJ}) to shape the injected current, which will be referred to as the reference topology (Ref). Capacitance and inductance have to be selected such that the peak current of the LC circuit exceeds the maximum fault current by a defined safety margin. A high resonance frequency of the circuit is beneficial, since component size and thus costs are smaller as well as the time to current zero. Limiting factor is the interruption capability of the MCB, i.e. gradients of current before and voltage after zero crossing. For low (fault) currents, current zero is reached earlier and with a higher gradient, increasing RRC_{CZ-}. Additionally, the charge remaining in the injection capacitor is higher, leading to higher RRC_{CZ+} as well as a higher peak transient interruption voltage. Both make it more difficult for the MCB to interrupt the current at zero crossing and often set a lower limit for the smallest current that can be switched successfully.

The improved injection circuit (Imp) consists only of the pre-charge injection capacitor in the CCP and the SI (as well as a small SA) in the NCP (black and orange components in Fig. 15). This makes it possible to have a lower inductance compared to the reference topology at the beginning of the injection, when a fast build-up of the injection current is required. Additionally, the inductance of the circuit close to current zero crossing in the MCB is considerably higher than in the reference topology, leading to a decreased RRC_{CZ-}, facilitating successful interruption.

For the dimensioning of the discussed topologies, a terminal fault in a 320 kV system with 100 mH current limiting inductance serves as reference. The dimensioning of the reference injection topology is done as described in [8, 31]. The key parameters of the study are summarised in Table 2. The SI is designed using the formulas presented in Section 4. In saturation state, the inductance is selected to be similar to the linear inductance in the reference injection circuit. By introducing a sufficiently large air gap in the core, a trade-off between high non-saturated inductance and high saturation current can be found. In this case, a Δt of 25 μs is aimed for based on findings in [32] (high voltage GCB), leading to a saturation current of 206 A and a non-saturated inductance of 36.6 mH. To investigate the maximum occurring stresses at interruption, the MCB is modelled by an ideal switch.

6.2 Simulation results

Fig. 16 illustrates simulated currents and voltages of the interruption process for the reference and the improved injection topology for representative high (HighF) and low fault current levels (LowF) to interrupt. After detection of the fault, the MCB is signalled to open. Once it reaches a sufficient contact distance to withstand the recovery voltage, a counter current is injected from the CCP to create a zero crossing in the MCB, at which it clears. The fault current commutates into the CCP, where it charges the injection capacitor to the clamping voltage of the SA. This is followed by a commutation of the fault current into the EAP and a dissipation of inductive energy stored in the system.

For the interruption process in the MCB, the current slope before zero crossing in the NCP (RRC_{CZ-}) and the subsequent voltage rise (RRC_{CZ+}) are of importance (close-up of the respective phase in the simulation is depicted in Fig. 17). Here, the differences between the topologies become apparent. Fig. 18

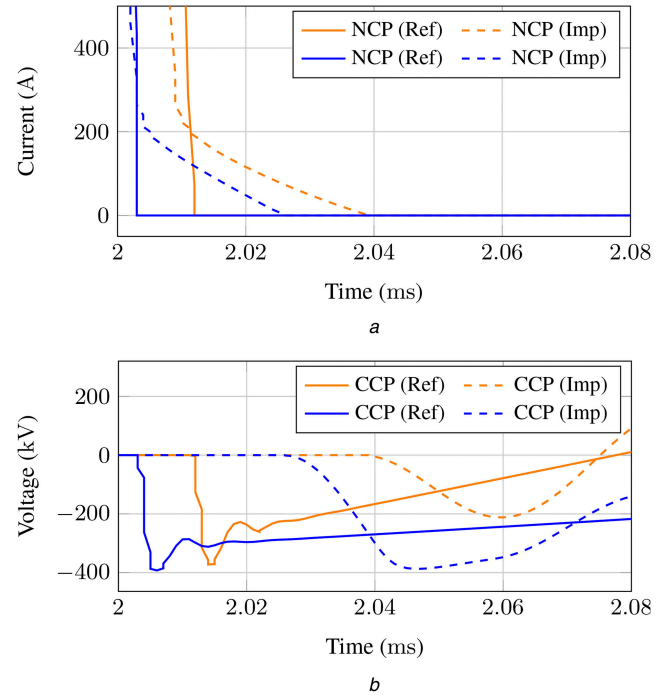**Table 2** Components of the circuit breaker topologies

Component	Value
system	
V_{DC}	320 kV
L_{DC}	100 mH
injection circuits	
C_{INJ}	1.7 μF
linear inductor	
L_{INJ}	500 μH

| Component	Value
SI	
N	70
A_E	0.06 m^2
δ	1 cm
B_S	1.8 T
l_E	1 m
$L_{non-sat}$	36.6 mH
L_{sat}	365 μH
SA_{MCB}	
$U_{SAMCBmax}$	600 kV
$I_{SAMCBmax}$	0.2 kA
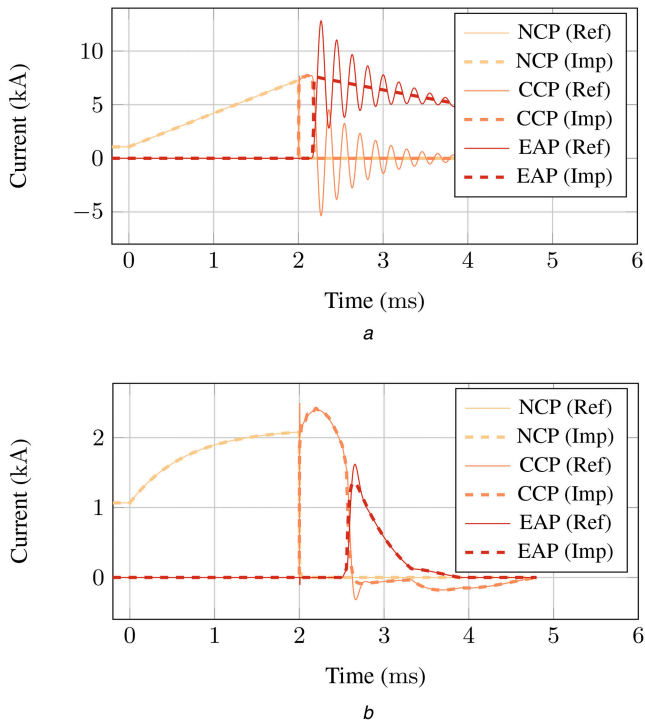
Fig. 16 Simulation of fault current interruption for HVDC with reference (Ref, solid) and improved injection topology (Imp, dashed)
(a) Simulation of interrupting a high fault current (HighF), *(b)* Simulation of interrupting a low fault current (LowF)

Fig. 17 Close-up of Fig. 16: simulation of fault current interruption for HVDC with reference (Ref, solid) and improved topology (Impr, dashed) for low (LowF, red) and high (HighF, blue) fault currents
(a) Current traces around zero crossing, *(b)* Voltage traces around zero crossing
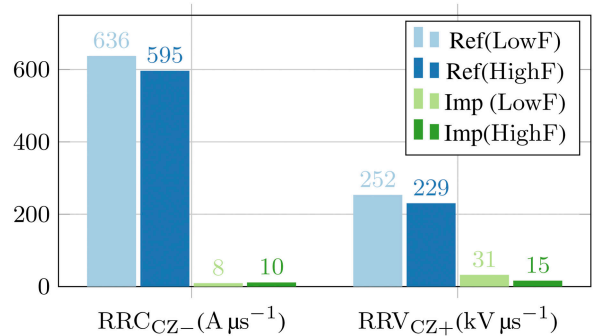
Fig. 18 Comparison of simulated rates of rise of current and voltage at zero crossing for reference (Ref) and improved injection topology (Imp) for high (HighF) and low fault current (LowF)

illustrates current and voltage gradient and clearly shows that the reference topology is likely to exceed interruption limits even for a stack of vacuum interrupters, due to the high frequency injection circuit. The use of a SI leads to a drastic decrease in current slope shortly before zero crossing. In this case, even with a relatively small air-gaped core, the rate of rise can be reduced by two orders of magnitude from the saturated to the non-saturated state for 20–30 μs. Compared to the dimensioning of the reference topology, this will considerably reduce the stresses for the MCB during interruption, ensuring a successful switching operation. While a re-dimensioning of the reference topology to reach lower gradients at zero crossing for successful interruption at low fault currents is possible, this will reduce the peak interruption current. Keeping peak injection current constant while decreasing RRC$_{CZ-}$ by a certain factor would result in similar increases in L and C, increasing the overall cost and operation time. A two order of magnitude increase consequently does not seem feasible.

Besides current before zero crossing, the SI also impacts the initial transient interruption voltage (ITIV), especially the RRC$_{CZ+}$. Due to the additional inductance, the rates at the improved injection circuit are about two orders of magnitude lower than for the reference (cf. Fig. 18). Additionally, the period of low current gradient delays the current zero crossing. This leads to a further discharge of the injection capacitor and thus a decrease in ITIV peak compared to the reference topology. This effect becomes more pronounced at high fault currents, as the rate of change of injection capacitor voltage is highest close to peak injection current. For small fault currents, the effect is negligible. On the contrary, when the injection capacitor is still almost completely charged at current zero in the NCP due to small fault currents, the peak voltage across the MCB could even exceed the one of the reference topology. This is due to the fact that the main SA in the EAP is connected to both MCB and SI. A negative voltage drop across the SI during ITIV build-up thus results in higher voltages

across the MCB, before the SA clamping voltage is reached. This problem can be solved by adding a small additional SA across the MCB (cf. Fig. 15), which is able to limit the overvoltage. To ensure that the SA does not share duties with the SA in the EAP, absorbing the energy stored in the grid inductances, its residual voltage needs to be higher than that of SA_{EAP}. As the absorbed energy is rather small (single digit kilo joule), the costs of such a surge arrestor can be considered minor. As the SA is a critical component, a sufficient safety margin should be included in the dimensioning process and redundancy considered.

For the higher fault current HighF, the reference topology shows a strong oscillation between CCP and EAP. As the MCB interrupts the current flow in the NCP, the energy stored in the injection inductor has to be dissipated in the SA of the EAP. This is not the case in the improved injection topology, as there is no additional inductance in the CCP, leading to reduced stresses for the SA.

During nominal operation, the SI will create additional conduction and magnetisation losses as it is in the NCP. However, with sufficient conductor cross-section, the ohmic losses can be considered negligible due to the limited number of windings. Magnetisation losses occur due to ripple in the DC system, which depend on the specific grid [33]. However, as the saturation current is very low compared to typical load currents, the device will be in saturation for normal operation and thus losses due to changes in magnetic flux are expected to be negligible as well.

7 Conclusion

MCBs are the key component of current injection type HVDC circuit breakers. To reduce size and cost of the circuit breaker topology, high-frequency injection circuits are beneficial. However, this is limited by the interruption performance of MCBs, which is a function of rate of rise of current before and rate of voltage after current zero crossing. To improve the interruption performance of MCBs, the current gradient can be reduced shortly before current zero crossing by the use of a SI.

In this paper, the influence of this period of low current gradient on the interruption performance of GCBs is investigated. After a determination of arc time constant and interruption performance for constant current and voltage gradients around zero crossing, it is shown that these parameters are sufficient to determine an optimal period of low current gradient and dimension a corresponding SI. Using this inductor, it was possible to decrease the rate of rise of current at zero crossing in the MCB considerably. Prospective currents of more than twice the maximum interruptable rate of rise of current have been successfully interrupted without indication of problems for further improvement. Consequently, controlling the pre-current-zero current shape appears to be highly promising for optimising current injection circuit breaker topologies.

A simulation study of a reference current injection topology and an improved topology based on a SI show the feasibility for the use in HVDC systems. With the improved injection topology, it appears possible to reduce rates of rise of current before and voltage after current zero crossing by two orders of magnitude. For a given interruption performance of a MCB, the passive components of the injection circuit can be minimised, making the system considerably more economical. Additionally, reducing the required interruption performance for the MCB can make it possible to use a single GCB instead of a series connection of multiple VCBs, requiring a more complex drive and equal voltage distribution, if it can be operated sufficiently fast.

8 Acknowledgment

9 References

[1] Franck, C.M.: 'HVDC circuit breakers: a review identifying future research needs', *IEEE Trans. Power Deliv.*, 2011, **26**, (2), pp. 998–1007

[2] Franck, C.M., Smeets, R.: 'Technical requirements and specifications of state-of-the-art HVDC switching equipment'. Cigré Technical Brochure 683, 2017

[3] Greenwood, A.N., Lee, T.H.: 'Theory and application of the commutation principle for HVDC circuit breakers', *IEEE Trans. Power Appar. Syst.*, 1972, **PAS-91**, (4), pp. 1570–1574

[4] Senda, T., Tamagawa, T., Higuchi, K., *et al.*: 'Development of HVDC circuit breaker based on hybrid interruption scheme', *IEEE Trans. Power Appar. Syst.*, 1984, **PAS-103**, (3), pp. 545–552

[5] Callavik, M., Blomberg, A.: 'The hybrid HVDC breaker an innovation breakthrough enabling reliable HVDC grids', *ABB Grid Syst. Tech. Pap.*, 2012, **361**, pp. 143–152

[6] Grieshaber, W., Dupraz, J., Penache, D., *et al.*: 'Development and test of a 120 kv direct current circuit breaker'. Proc. CIGRÉ Session, Paris, France, 2014, pp. 1–11

[7] Kontos, E., Schultz, T., Mackay, L., *et al.*: 'Multiline breaker for HVDC applications', *IEEE Trans. Power Deliv.*, 2018, **33**, (3), pp. 1469–1478

[8] Lenz, V., Schultz, T., Franck, C.M.: 'Impact of topology and fault current on dimensioning and performance of HVDC circuit breakers'. 2017 4th Int. Conf. on Electric Power Equipment – Switching Technology, ICEPE-ST 2017, Xi'an, China, 2017, pp. 356–364

[9] Greenwood, A., Barkan, P., Kracht, W.C.: 'HVDC vacuum circuit breakers', *IEEE Trans. Power Appar. Syst.*, 1972, **PAS-91**, (4), pp. 1575–1588

[10] Wang, Y., Marquardt, R.: 'Performance of a new fast switching DC-breaker for meshed HVDC-grids'. 17th European Conf. on Power Electronics and Applications, Geneva, Switzerland, 2015, pp. 1–9

[11] Yao, X., Wang, J., Geng, Y., *et al.*: 'Development and type test of a single-break 126-kV/40-kA–2500-A vacuum circuit breaker', 2016, **31**, (1), pp. 182–190

[12] Zhang, Y., Yao, X., Liu, Z., *et al.*: 'Axial magnetic field strength needed for a 126-kV single-break vacuum circuit breaker during asymmetrical current switching', 2013, **41**, (6), pp. 1670–1678

[13] Anderson, J.M., Carroll, J.J.: 'Applicability of a vacuum interrupter as the basic switch element in HVDC breakers', *IEEE Trans. Power Appar. Syst.*, 1978, **PAS-97**, (5), pp. 1893–1900

[14] Yanabu, S., Kaneko, E., Tamagawa, T., *et al.*: '真空しゃ断器の直流大電流しゃ断特性', *IEEJ Trans. Power Energy*, 1980, **100**, (11), pp. 649–656

[15] Premerlani, W.J.: 'Forced commutation performance of vacuum switches for HVDC breaker application', *IEEE Power Eng. Rev.*, 1982, **PER-2**, (8), pp. 46–46

[16] Gorman, J.G., Kimblin, C.W., Voshall, R.E., *et al.*: 'The interaction of vacuum arcs with magnetic fields and applications', *IEEE Power Eng. Rev.*, 1983, **PER-3**, (2), pp. 19–19

[17] Niwa, Y., Yokokura, K., Matsuzaki, J.: 'Fundamental investigation and application of high-speed VCB for DC power system of railway'. 24th ISDEIV 2010. IEEE, Braunschweig, Germany, 2010, vol. 1, pp. 125–128

[18] Tokoyoda, S., Sato, M., Kamei, K., *et al.*: 'High frequency interruption characteristics of VCB and its application to high voltage DC circuit breaker'. 2015 3rd Int. Conf. on Electric Power Equipment – Switching Technology (ICEPE-ST), Busan, South Korea, 2015, pp. 117–121

[19] Cao, L.J., Stokes, A.D.: 'Ablation arc. III. Time constants of ablation-stabilized arcs in PTFE and ice', *J. Phys. D, Appl. Phys.*, 1991, **24**, (9), pp. 1557–1562

[20] Chapman, A., Jones, G.R.: 'The local electrical properties of gas blast arcs near current zero', *IEEE Trans. Plasma Sci.*, 1978, **6**, (3), pp. 300–313

[21] Ragaller, K. (Ed.): 'Current interruption in high-voltage networks' (Springer US, Boston, MA, 1978)

[22] Frind, G., Rich, J.: 'Recovery speed of axial flow gas blast interrupter: dependence on pressure and dI/dt for air anf SF6', *IEEE Trans. Power Appar. Syst.*, 1974, **PAS-93**, (5), pp. 1675–1684

[23] Schultz, T., Franck, C.M.: 'Interruption capability investigations of a model gas circuit-breaker for HVDC switching applications'. Int. Conf. on Gas Discharge and their Applications, Nagoya, Japan, 2016, pp. 173–176

[24] Walter, M.M.: 'Switching arcs in passive resonance HVDC circuit breakers', ETH Zurich, 2013

[25] Ritter, A., Bort, L.S.J., Franck, C.M.: 'Five years of pulsed current testing for HVDC switchgear'. 2016 IEEE Int. Conf. on High Voltage Engineering and Application (ICHVE), Chengdu, China, 2016, pp. 1–4

[26] Mayr, O.: 'Beiträge zur Theorie des statischen und des dynamischen Lichtbogens', *Arch. Elektrotech.*, 1943, **64**, pp. 588–608

[27] Jones, G.R.: 'High pressure arcs: introduction & electrical diagnostics' (Cambridge University Press, Cambridge, UK, 1988)

[28] Garzon, R.: 'High voltage circuit breakers: design and applications' (Marcel Dekker, New York, NY, USA, 2002)

[29] Urai, H., Ooshita, Y., Koizumi, M., *et al.*: 'Estimation of 80 kA short-line fault interrupting capability in an SF6 gas circuit breaker based on arc model calculation'. 17th International Conference on Gas Discharges and Their Applications, Cardiff, UK, 2009, pp. 129–132

[30] Knobloch, H.: 'ARC resistance at current zero: a tool to describe the breaking capacity of SF'. 11th Int. Symp. on High-Voltage Engineering (ISH 99), London, UK, 1999, vol. 1999, pp. v3–205–v3–205

[31] Schultz, T., Lenz, V., Franck, C.M.: 'Circuit breakers for fault current interruption in HVDC grids'. VDE-Fachtagung Hochspannungstechnik, Berlin, Germany, November 2016, pp. 1–6

[32] Frind, G.: 'Experimental investigation of limiting curves for current interruption of gas blast breakers', in Ragaller, K. (Ed): 'Current interruption in high-voltage networks' (Springer, Boston, MA, USA, 1977), pp. 67–94

[33] IEC: 'High-voltage direct current (HVDC) power transmission using voltage sourced converters (VSC)'. IEC TR 62543, 2013